International Journal of Heat and Mass Transfer 52 (2009) 301–308

Contents lists available at ScienceDirect

International Journal of Heat and Mass Transfer

journal homepage: www.elsevier.com/locate/ijhmt

Loop heat pipe for cooling of high-power electronic components

Leonid Vasiliev [a,*], David Lossouarn [b], Cyril Romestant [b], Alain Alexandre [b], Yves Bertin [b], Yauheni Piatsiushyk [c], Vladimir Romanenkov [c]

[a] Luikov Heat and Mass Transfer Institute, 220072, 15, P. Brovka Strasse, Minsk, Belarus
[b] LET, UMR-CNRS-ENSMA 6608, 1 Avenue Clément Ader, Futuroscope, France
[c] Belarusian National Technical University, 220107, 77, Partizansky Avenue, Minsk, Belarus

ARTICLE INFO

Article history:
Received 11 October 2007
Received in revised form 3 June 2008
Available online 3 August 2008

Keywords:
Loop heat pipe
Wick structure
Evaporation
Heat transfer

ABSTRACT

In this paper, we present a new development of loop heat pipe (LHP) technology in its applications to cooling systems for high-power IGBT elements. An advanced method of LHP evaporator wick manufacturing has been proposed. Following this approach, a 16 mm outer diameter and 280 mm-length LHP evaporator was designed and manufactured. Nickel and titanium particles were used as raw material in LHP evaporator wick fabrication. LHP with a nominal capacity as high as 900 W for steady-state condition and more than 900 W for a periodic mode of operation at a temperature level below 100 °C and a heat transfer distance of 1.5 m was designed through the cooling of a high-power electronic module. An experimental program was developed to execute LHP performance tests and monitor its operability over a span of time. An investigation of the effects of LHP performance of parameters such as evaporator and condenser temperatures and LHP orientation in a gravity field was brought about. As regards the results of this initial series of tests, it was found that LHP spatial orientation within the nominal range of heat loads has no drastic effect on overall LHP functioning, whereas condenser temperature does play an important role, especially in the range of heat load close to critical. A 2D nodal model of the evaporator was developed and provides us with confirmation of the suggestion that when high-power dissipation levels are available, low wick conductivity is well adapted for LHP applications.

1. Introduction

Presently there exist two widely used cooling modes for high-power semiconductor components (IGBT, IGHTs and other modules). A low efficiency level, the need to use a liquid pump, and pollution and incrustation of working fluid are the main drawbacks of single-phase cooling systems. Another disadvantage of liquid cooling systems, especially in transport applications such as trains and electrocars, consists in the large mass of working fluid due to the liquid's inertia during the acceleration and braking phases.

As for heat pipe-based heat exchangers, they present greater overall efficiency as well as a low mass of working fluid [1,2]. Another major advantage of a heat pipe is that it furnishes a totally passive mode in transmission of heat from hot electronic components to released area into the atmosphere. The reader may be reminded that a heat pipe is a sealed metallic container containing a capillary wick suffused with a small amount of working fluid. This latter is at the saturation state so that it vaporizes as heat is applied to the heat pipe envelope or condensate as heat is removed. Due to saturation pressure difference, the vapor emanating from the heat pipe evaporator moves to the condenser where it condenses and releases its latent heat energy, which is absorbed by the surroundings. The wick structure in the heat pipe's inner wall provides capillary forces that pump the condensate back to the hot end of the heat pipe and thereby complete the continuous evaporation/condensation cycle.

Two-phase loop with capillary pump (LHP) is a variety of heat pipe in which the evaporator and the condenser are separated, with the working fluid being transported between the two components via tubing or pipes [3–5]. Along with its high cooling capability, this type of flexible design renders LHP a highly promising candidate for advanced cooling systems in modern high-power electronic modules.

Generally speaking, the LHP evaporators present a cylindrical shape with a 12–28 mm diameter and a length/diameter ratio ranging from 5 to 10 [6] on account of the technical difficulties of porous structure realization that impinging upon evaporator performances. In many applications, especially when the length/diameter ratio is greater than 10, it is desirable that the thermal management system assure uniformly high rates of heat removal over a larger area. In this paper, an experimental investigation of LHP with an evaporator length/diameter ratio of close to 18 is to be presented (Fig. 1).

* Corresponding author. Tel.: +375172842139; fax: +375172842133.
E-mail addresses: L.Vasiliev@rambler.ru, leonid.l.vasiliev.jr@gmail.com (L. Vasiliev).

0017-9310/$ - see front matter © 2008 Elsevier Ltd. All rights reserved.
doi:10.1016/j.ijheatmasstransfer.2008.06.016

Nomenclature

G	thermal conductance (W K^{-1})	λ	effective conductivity (W m^{-1} K^{-1})
l_v	latent heat (J kg^{-1})	θ	opening angle of the node (rad)
L	node length (m)	μ	liquid dynamic viscosity (Pa s)
M	molecular mass (kg mol^{-1})	ρ	density (kg m^{-3})
Q	power of heat flux (W)		
R	node internal or external radius (m)	*Subscripts*	
S	node exchange surface (m^2)	if	interface
T	temperature (K)	sat	saturation
		vap	vapor
Greek letters			
α	evaporation coefficient		

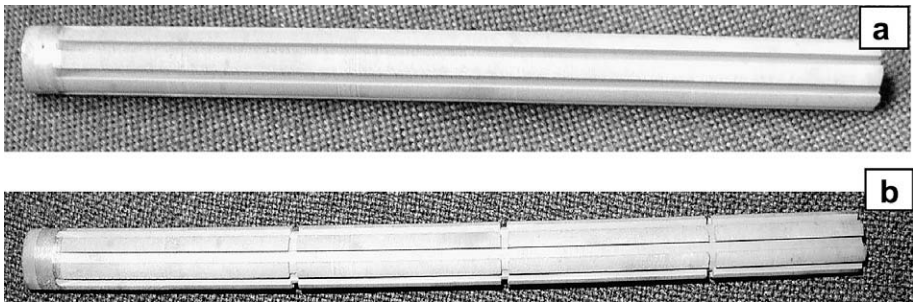

Fig. 1. Photo of LHP evaporator wick. (a) With longitude grooves only; (b) with longitude and transversal grooves.

2. Advanced LHP wick design

Traditional fabrication process of LHP evaporator consists of four main operations: pressing metal powder in a specially designed tool, the sintering process, creation of vapor removal grooves on the wick structure's outer surface, and introduction of the wick structure in a metal envelope.

We wish to propose a new technology for the pressing process in which the pressing metal particles are preliminarily introduced into the soft polymer matrices. Application of the soft (polymer-based) envelope (Fig. 2) along with a radial mode of mechanical pressure (Fig. 3) constitute an advanced method of metal powder treatment ensuring uniform pore distribution and wick density subsequent to pressing throughout the wick.

A good uniformity of the thermophysical properties of porous structure and needed uniform porosity in large porous values range of whole volume of the wick is ensured (Fig. 4).

Since this technology allows for creation of vapor removal grooves simultaneously with metal particle compression, it is less costly than mechanical wick cutting and electro-erosion treatment.

Another major advantage of the proposed metal particle pressing procedures is that they entail no need to apply the vacuum press form, as is customarily done in conventional hydraulic pressing technology.

3. Wick structure hydraulic analysis

It is a well-known fact that in LHP pressure balance, loss of pressure through the wick is a significant factor. Wick permeability K is in direct correlation with wick structure porosity ε, which is defined as the ratio of pore volume to total volume of the wick, and is usually given by:

$$K = \frac{2\varepsilon r_h^2}{f_l Re_l}, \tag{1}$$

where (f_l) is the friction factor. Given the typically small size of the porous structure's hydraulic radius along with a typically low liquid flow velocity, the liquid flow may be considered laminar. Hence, the values of ($f_l Re_l$) depend only on flow passage shape and can likewise be deemed constant. Such an assumption is basically valid as regards homogeneous porous structures.

Review of the literature shows that most researches have focused on the thermal and hydraulic properties of wick structure in macroscopic point of view. But, in the design of LHP evaporators, vapor removal grooves are found on the outer surface of the wick, which structure of the surface is typically deformed. The degree of deformation hinging upon the mode of groove creation. Due to the convenience of their mechanical and thermal properties, Ni- and Ti-based wick structures are widely used in LHP evaporator fabrication.

In this work, the grooved surface of the wick structure resulting from mechanical treatment, electro-erosion technology and from the powder pressing into the soft polymer matrix and rigid metallic press forms has been submitted to close investigation. Photos of the Ni-sintered wicks for which the vapor removal grooves were created by these different techniques are shown in Fig. 5. The photos were obtained through use of the scanning electron microscope Nanolab-7 (Opton, Germany). Stereological analysis of groove surfaces was performed with the help of the automatic picture analyzer known as "Mini-Magiscan" ("Joyce Loebl", UK) and the "Genias 26" software.

Analysis results attest to the following:

(1) During electro-erosion treatment, some of the metal particles partially melt, and their evaporation stimulates a further procedure of vapor/liquid/crystal formation. As an additional consequence of this application, the range of particle diameters on the wick surface widens, while the range of pore diameters is in no way uniform. Moreover, it is difficult to compare a porous wick surface with a wick surface subsequent to mechanical cutting of the latter. Finally, electro-erosion treat-

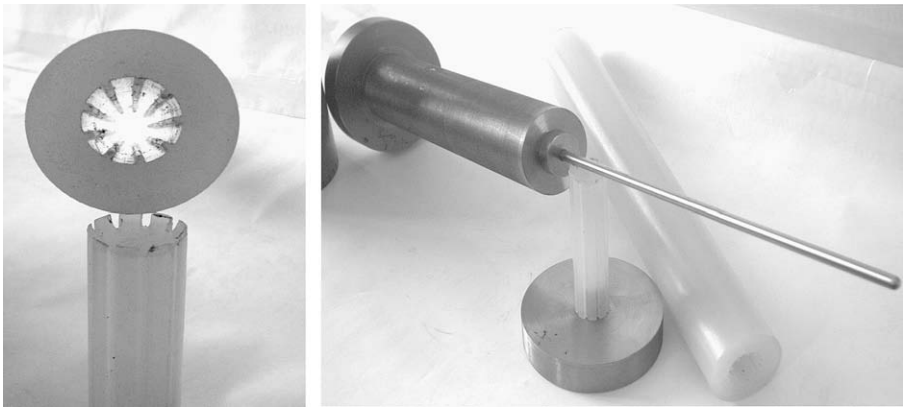

Fig. 2. Photo of original set-up for metal powder pressing in soft polymer matrix.

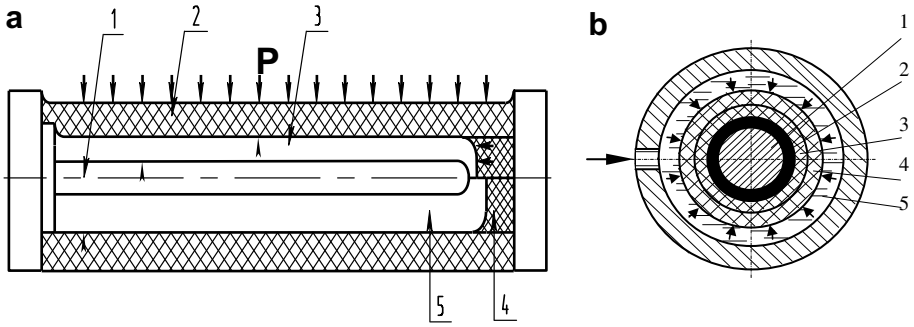

Fig. 3. (a) Longitudinal section scheme of the set-up for pressing of metal powder; (b) cross-section scheme of the set-up for pressing of metal powder: 1 – central matrix; 2 – metal powder; 3 and 4 – soft polymer matrixes; and 5 – liquid.

ment of the porous structure increases surface pore diameter up to 10–15 μm, and decreases surface porosity (quantity of open pores) down to 25% (Figs. 5a and 6).

(2) The tool's mechanical cutting of the wick grooves and pressing in the rigid metallic press are the reasons for the partially closed pore surface occasioned by deformation of the wick. Use of these traditional technologies likewise explains reduction of pore diameter on the wick surface and the permeability of the porous structure. In fact, mean pore diameter after mechanical cutting of porous structure is decreased to 1.5 μm, while surface porosity goes down to 27% with mechanical treatment and to 23% with pressing in a metallic press form (Figs. 5b, c, 6 and 7).

(3) A much more satisfactorily smooth and uniform surface of the wick was achieved when we applied the new technology with metal powder pressing into the soft polymer matrix. The wick surface, we successfully obtained, presents uniformly open-type pore distribution along with maximal (35%) porosity of the wick structure. As for the level of non-uniformity in the volumetric porous structure, it remains within a 3% limit (Figs. 5d and 8).

4. LHP evaporator model

In order to assess the way through which heat flux is distributed over a porous wick, a numerical model was developed using a nodal method. A steady-state source of heat flow dissipation is considered in our estimates of the degree of subcooling required to ensure satisfactory LHP functioning. Given the evaporator's cylindrical shape, it can be usefully divided into elementary patterns consisting in circumferential body layers, half a tooth of porous wick, half a vapor groove, and the body of the wick (Fig. 9).

The model is bi-dimensional with uniform heat flow distribution along the evaporator.

We have taken into consideration the association of two parallel networks as described by the following equations:

$$\dot{Q}_{j,j+1} = \frac{\lambda L \ln(R_{k+1}/R_k)}{\theta}(T_{j+1,k} - T_{j,k}) \tag{2}$$

$$\dot{Q}_{k,k+1} = \frac{\lambda \theta L}{\ln(R_{k+1}/R_k)}(T_{j,k+1} - T_{j,k}) \tag{3}$$

$$\dot{m}_{j,j+1} = \frac{\rho(T_{j,k})}{\mu(T_{j,k})}\kappa\frac{S_k}{L_{j,j+1}}(p_{j+1,k} - p_{j,k}) \tag{4}$$

$$\dot{m}_{k,k+1} = \frac{\rho(T_{j,k})}{\mu(T_{j,k})}\kappa\frac{S_j}{L_{k,k+1}}(p_{j,k+1} - p_{j,k}) \tag{5}$$

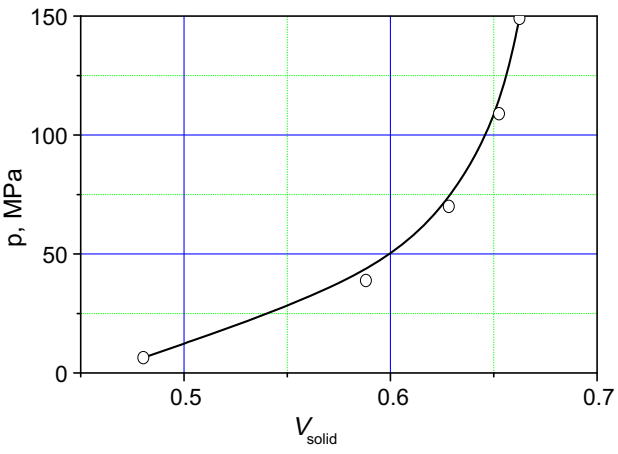

Fig. 4. Volume of Ni pressed powder ($V_{solid} = V_{tot} - V_{pore}$) vs. applying pressure level.

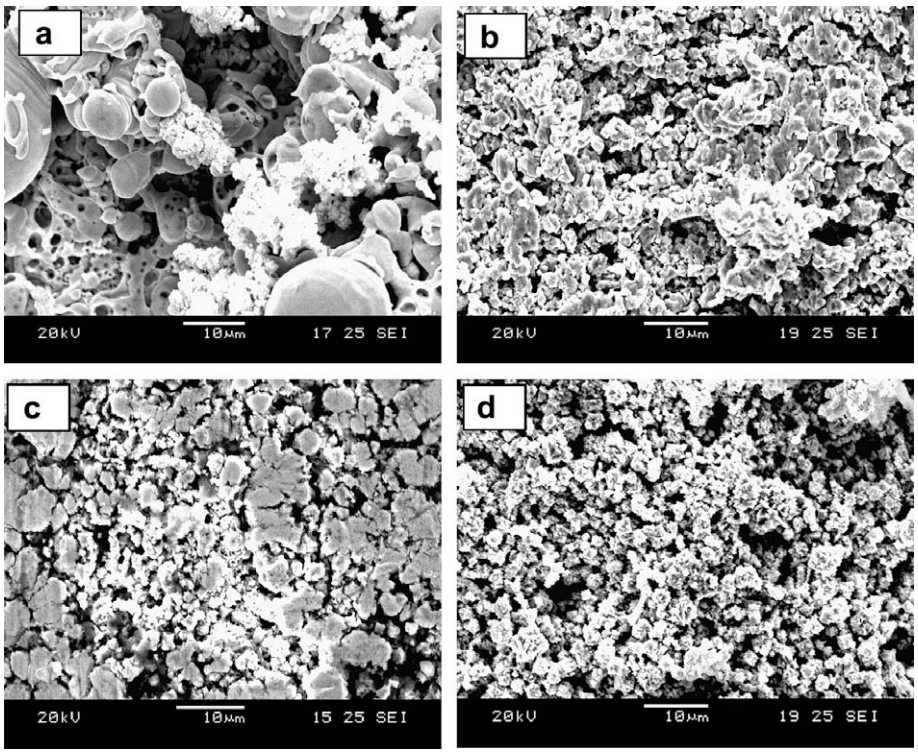

Fig. 5. Photos of grooved porous surfaces made by: (a) electro-erosion; (b) mechanical treatment; (c) pressing in the rigid press form; and (d) pressing into soft press form.

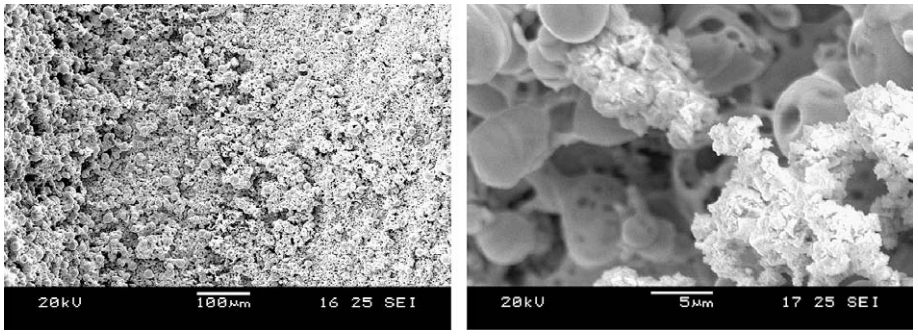

Fig. 6. Photos of grooved porous surface made by electro-erosion.

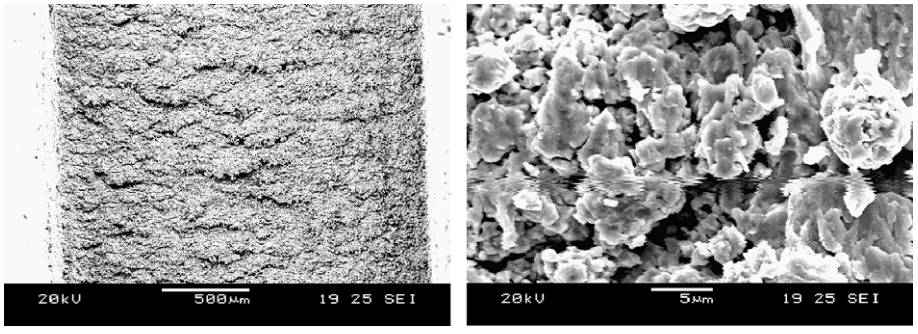

Fig. 7. Photos of grooved porous surface made by mechanical treatment.

In the first network (Eqs. (2) and (3)), the thermal nodes are connected to each other through couplings determined by geometry and thermophysical properties. In the second network (Eqs. (4) and (5)), pressure nodes constitute a hydraulic model depicting mass flow rates.

The boundary conditions are set as follows: the vapor is assumed to be overheated and its temperature is equal to the temperature measured at the evaporator's outlet. After that, the heat removed from the evaporator is quantified in terms of the temperature difference between vapor–liquid

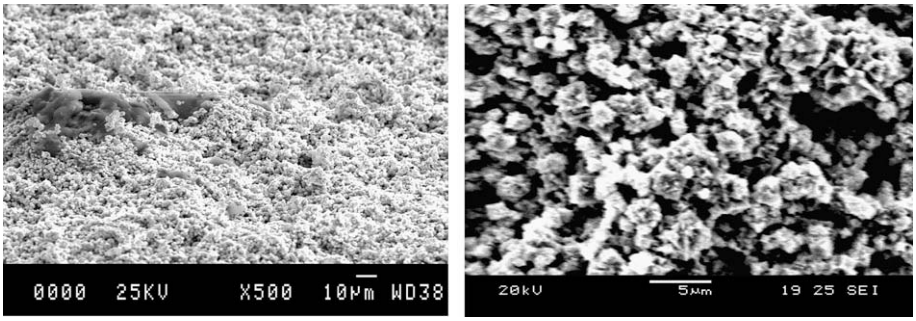

Fig. 8. Photos of grooved porous surface made by pressing into soft matrix.

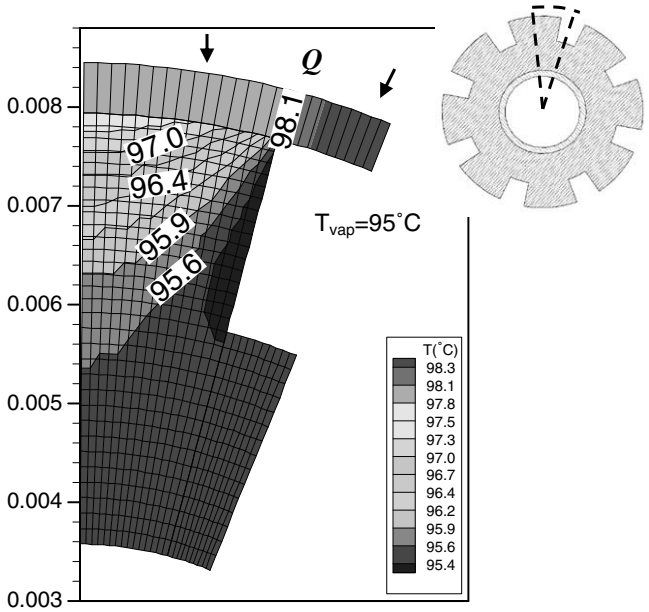

Fig. 9. Isothermal curves on elementary pattern.

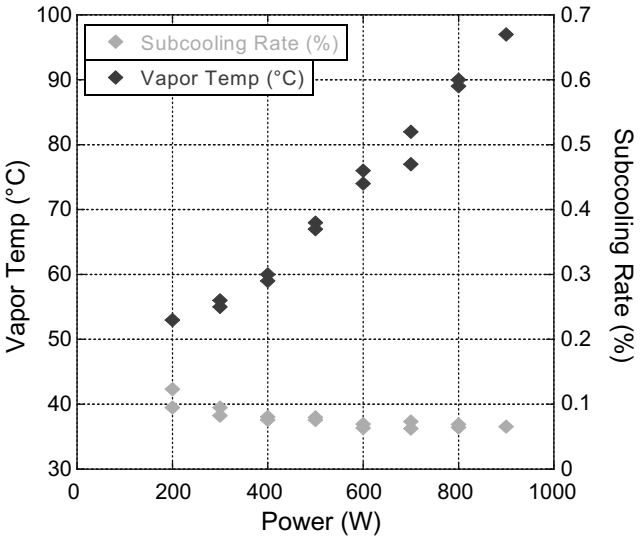

Fig. 10. Subcooling rate vs. heat power for steady-state conditions.

interface multiplied by evaporator conductance. In the final analysis, the mass flow rate at the interface is deduced from total heat removed and vaporization enthalpy under saturation conditions:

$$T_{vap} = T_{vap\ essai}\dot{Q}_{if} = G_{ev}(T_{vap} - T_{if})$$
$$\dot{m}_{if,vap} = \dot{Q}_{if}/l_v(T_{sat}) \quad (6)$$

A key objective of the model is to evaluate the subcooling rate registered in the LHP for given vapor temperatures and for subcooled liquid temperatures in the liquid core of the evaporator. Evaporation conductance ( ) is calculated using the Hertz–Knudsen–Schrage equation:

$$G_{ev} = \frac{2\alpha}{2-\alpha}\sqrt{\frac{M}{2\pi RT_{sat}}}\frac{l_v^2\rho_l\rho_v}{T_{sat}(\rho_l - \rho_v)} \quad (7)$$

"Subcooling" heat is the portion of heat input that reheats liquid up to the temperature of the compensation chamber under saturation conditions. Hence, this subcooling is necessary to maintain the steady state in the compensation chamber. The main shortcoming of the previous evaporators we tested, such as nickel wick, consisted in the high numerical value of the portion of heat flow directed to the compensation chamber through the porous structure and on account of which, the liquid boiling in that chamber may occurs and block the LHP.

A change in the porous material structure and its effective conductivity by a multiple of approximately two allowed for reduction of saturation temperature during tests of the LHP. Figs. 10 and 13–16 show that vapor temperature in LHP is directly linked to main power dissipation. In accordance with Fig. 10 data, subcooling heat is reduced to 0.1%, whereas in previous prototypes, the minimum value was 5%.

Thanks to such an exceptionally low degree of subcooling heat, loop performances are correspondingly highly enhanced. As a matter of fact, the boiling process in the compensation chamber eventuates at a very late stage, and the saturation temperature is quite low with regard to the level of injected heat flux. The 2D model obviously fails to take into account the heat flux conducted to the compensation chamber and its pronounced influence on thermal regulation.

5. Experimental set-up

The experimental set-up of the LHP is shown in Fig. 11. Our general objective was to determine the maximum heat transfer capacity as well as temperature distribution along the LHP for differing heat loads, condenser temperatures and testing positions.

In order to reproduce electronic thermal activity, the evaporator heating source was assured by electric heaters, which are controlled by a DC power supply, while heat removal was brought about by circulation of the liquid through a coaxial liquid cooling jacket in a condenser or with the help of an air heat exchanger. As for the recirculating thermostat, it was used so as to provide a

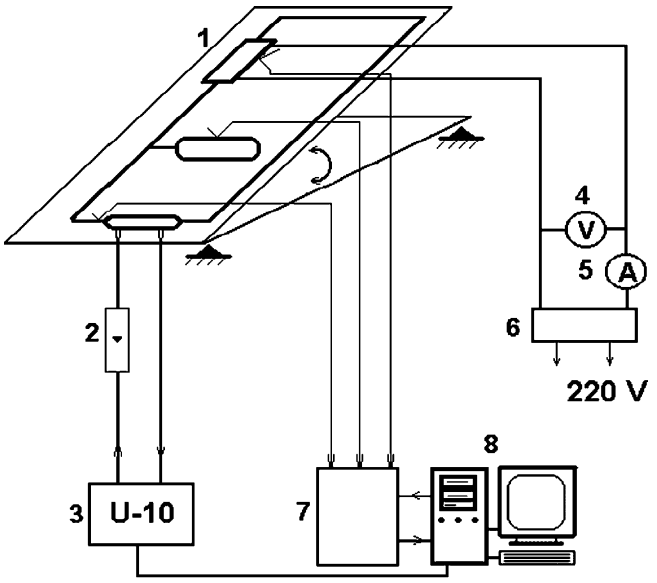

Fig. 11. Experimental set-up scheme: 1 – LHP on the platform responsible for the heat pipe inclination, 2 – rate sensor for liquid flow, 3 – thermostat, 4 – voltmeter, 5 – current sensor, 6 – electric source, 7 – Data Acquisition Unit, and 8 – PC.

Table 1
Geometrical and physical parameters of LHP

Evaporator/compensation chamber	
LHP evaporator	
Total length (mm)	334
Active length (mm)	280
Inner/outer diameters (mm)	16/18
Liquid accumulator	
Diameter/length	30/45
Material of metal envelope	Stainless steel
Working fluid	Water (acetone)
Porous wick	Titanium sintered powder
Mean pore diameter (μm)	5
Porosity	>55%
Thermal conductivity (W/(m K))	5–7
Porous wick	Nickel sintered powder
Mean pore diameter (μm)	5
Porosity	>55%
Thermal conductivity (W/(m K))	9–12
Liquid/vapor lines	
Length (mm)	1500
Outer/inner diameters (mm)	4/3; 6/5
Material	Stainless steel
Condenser	
Liquid heat exchangers	
Diameter/length (mm/mm)	5/560

continuous supply of cooling water and flow rate in areas where the coolant tank's temperature stability was controlled with an accuracy rate of ±1 °C. Evaporator heat load was applied in accordance with a computer program. The LHP was monitored by eight T-type thermocouples.

If there were two thermocouples on the outer surface of the compensation chamber (Fig. 12), this was because the CC was constantly subjected to two phase flow conditions. All the measured temperatures were transmitted to the computer through a Data Acquisition Switch Unit (Agilent 34970A) in real time, and were recorded once every 10 s for further analysis. Heat pipe tilt measurements were performed by a system of tilt regulation. The whole LHP remained thermally insulated for the duration of the tests. Water and high-grade acetone were used as a working fluid. Both the geometrical and the structural parameters of the LHP under investigation are presented in Table 1.

6. Analysis of experimental data

Three generations of LHP wicks made from Ni and Ti metal powder were tested under the same operational conditions. All of the wicks were of the same geometrical size, while the structural parameters were slightly different. The Ni and the Ti wicks presented nearly the same porosity, while the samples' thermal conductivity differed (Table 1). The diameters of longitudinal vapor removal grooves for the three types of LHP likewise differed. The

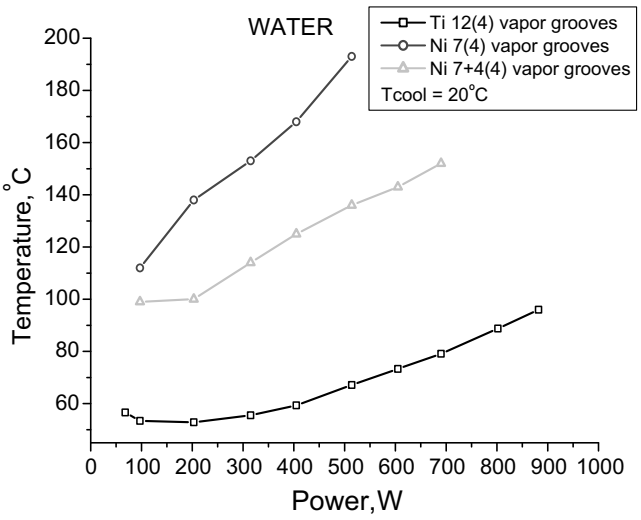

Fig. 13. Steady-state performance of LHP with Ti and Ni wicks at constant heating powers with water as working fluid.

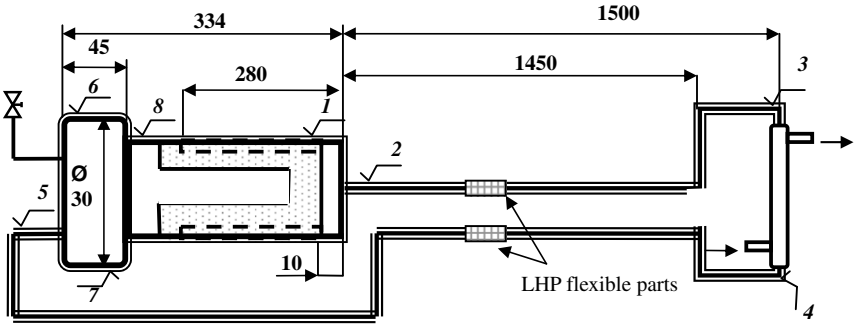

Fig. 12. A drawing of the LHP with location of the monitoring thermocouples (1–8).

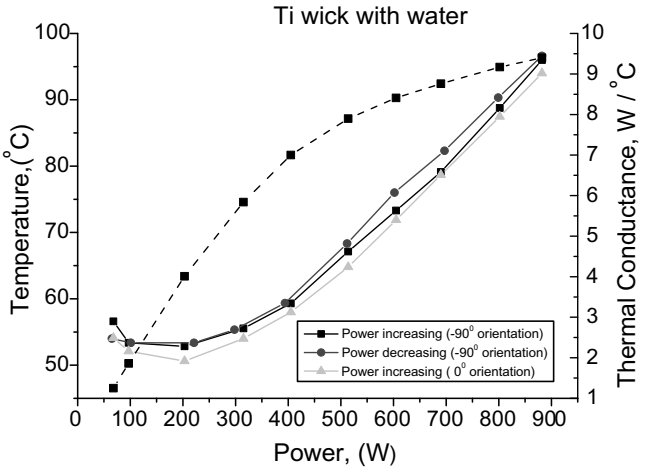

Fig. 14. Steady-state performance of LHP with Ti at different space orientations and constant heating powers and thermal conductance (dash lines) with water as working fluids.

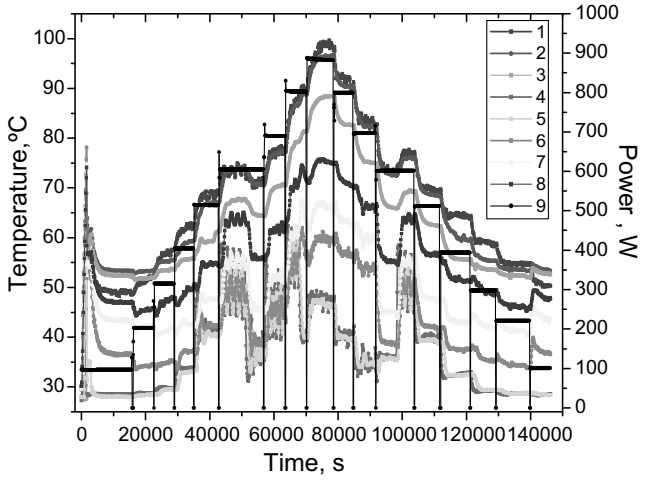

Fig. 16. Steady-state performance of LHP with Ti at constant heating powers with water as working fluids.

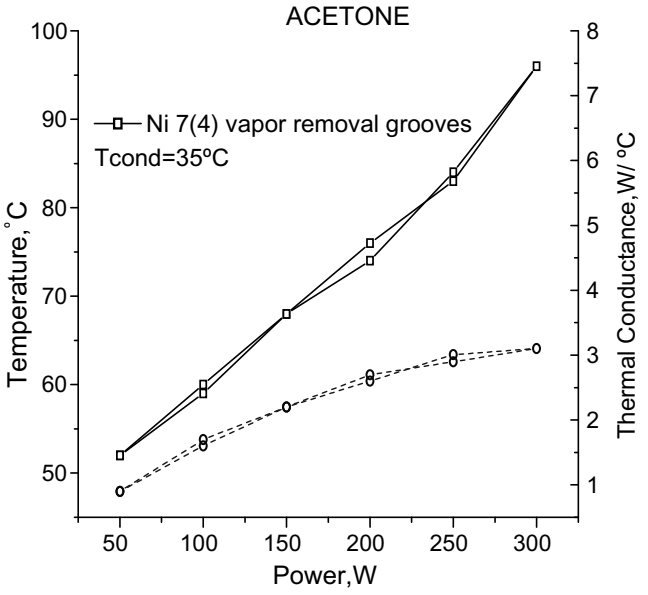

Fig. 15. Steady-state performance of LHP with Ni wick at constant heating powers and thermal conductance (dash lines) with acetone as a working fluid.

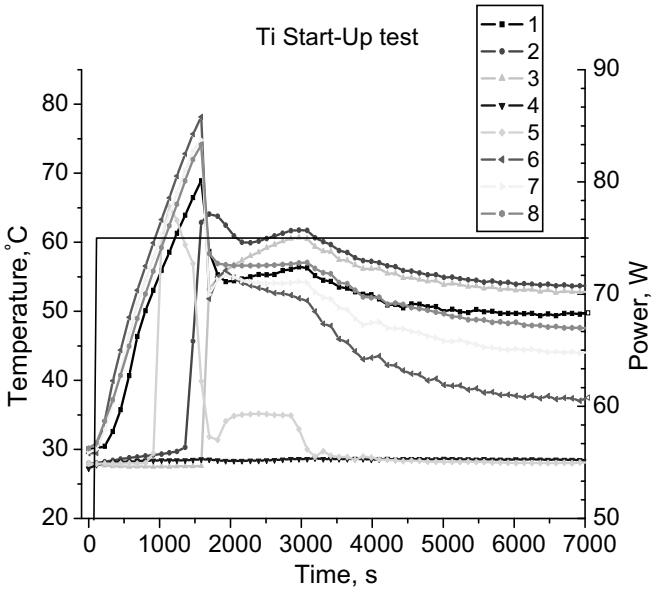

Fig. 17. LHP start-up tests.

first-generation Ni wicks had seven longitudinal grooves with 2 mm diameter. The second-generation Ni wicks also had seven longitudinal grooves, along with four additional grooves with 1.5 mm diameter. As for the last and third-generation wick, it had 12 longitudinal grooves with 2 mm diameter. All of the wicks featured four transverse vapor removal grooves. Temperature evolution of the LHP evaporator envelope as function of the heat load under steady-state conditions is shown in Figs. 13–15 for each of the three wicks tested. It is interesting to note that the Ti wick and the second-generation Ni wick (7 grooves + 4 grooves) are typical for LHP regions of constant and variable conductance (Fig. 13). Due to relatively high hydraulic resistance, the first-generation Ni wick definitely presents similarly higher thermal resistance.

Two sets of experiments with Ni and Ti wicks were performed to assess loop heat pipe cooling capability as well as temperature distribution along the LHP for different heat loads, condenser temperatures, and LHP testing positions as regards periodical and steady-state operation cycles.

For both sets of tests, a short coaxial liquid heat exchanger was used as a condenser. Temperature and liquid mass flow were regulated by a thermostat. With regard to fixed cooling conditions and spatial orientation, a step-by-step increasing and decreasing heat load was applied (steps of 100 W commencing with 100 W) so as to detect possible presence of hysteresis phenomena.

Figs. 14 and 16 show that the LHP with Ti wick and water as a working fluid transports up to 900 W for different spatial orientations and keeps the temperature of the heated wall lower than 100 °C, while with acetone as the LHP working fluid and a Ni wick, the maximal heat load did not exceed 300 W (Fig. 15). The latter is the maximum admissible temperature for electronic contact interface.

The flow rate of cooling water was kept the same throughout the first set of tests. It is important to note that the maximal cooling capability of the condenser liquid heat exchanger did not suffice in the final series of tests involving Ti wick. In order to maintain a constant temperature at the LHP condenser exit (Fig. 16), the liquid temperature in the condenser was changed

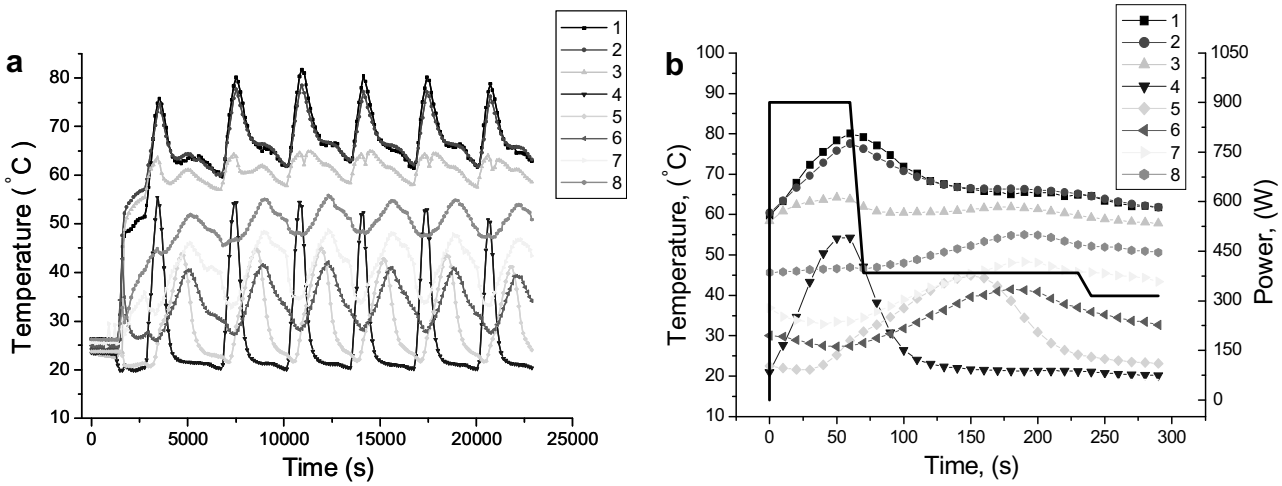

Fig. 18. Periodically steady operations with liquid heat exchangers (a); operation during one power supply cycle (b).

twice from 30 °C for heat loads ranging from 100 to 600 W to 20 °C for heat loads ranging from 600 to 900 W.

Fig. 17 demonstrates a typical LHP thermal profile at minimal heat load level (75 W) with regard to successful start-up conditions in a "worst case" situation (vertical orientation, evaporator top). At the time of LHP start-up, there occurs a temperature jump in the evaporator and compensation chamber until the heat transfer in the condenser fails to be stabilized (1650 s). Transient heat transfer in the condenser (liquid plug formation and its displacement to the CC) is completed after the aforementioned 1650 s time interval. The final steady-state condenser heat transfer constitutes the reason for the evaporator temperature decrease and its stabilization at 50 °C that is finally achieved.

The second set of tests with a liquid heat exchanger was performed so as to investigate LHP behavior for periodical heat loads. This series of experiments is of particular importance insofar as high-power electronic components (IGBT, IGHTs and others) are typically employed in transport applications associated with acceleration and braking. In these cases, it is necessary to guarantee adequate LHP functioning under actual operating conditions. The LHP cooling system need be reliable not only just for steady state, but also for periodical conditions of transport operation. The time interval for applied heat loads that was selected consequently corresponds to IGBT application in train electric drive (Fig. 18b). As can be observed in Fig. 18, maximum LHP evaporator temperature did not exceed 80 °C, which is nearly 20 °C lower than the maximum admissible temperature for electronic junction, whatever the test. During our tests, we regret to note that maximal heat load was limited by maximal electrical heater capability. This should be a worthwhile subject for further investigation. It also bears noting that during our tests, no liquid boiling occurred in the LHP compensation chamber.

7. Conclusions

A comprehensive investigation of the quality of the surface of sintered powder for loop heat pipe (LHP) evaporators was successfully conducted.

It was found that mean pore diameter as well as wick porosity on the surface of vapor removal grooves depend on the mode of wick, that is to say vapor groove fabrication.

New technology involving metal powder pressing into the soft matrix (i.e., the polymer envelope) provides a possibility to have the wick structured with the vapor removal grooves in the course of a single technical operation. As for treatment of the wick by mechanical pressure into the soft matrix, it not only in no way modified the wick's porous structure, but would also appear to allow for achievement of the needed porosity in a wide range of pore diameters; as a result, it may be constructively suggested in fabrication of LHP evaporator wick structure.

Prototypes of loop heat pipe for the cooling systems of high-power electronic modules have been designed, fabricated and tested with regard to high-heat flux transfer. These loops need be adapted to transient power dissipation as well as steady-state regimes. Following nickel porous wicks, titanium evaporators have been developed so as to enhance regulation of saturation temperature inside the loop. These most recent prototypes manifest high performance and are able to transfer over 1100 W for temperatures regulated below 100 °C in transient dissipation.

A 2D nodal model of the evaporator provides us with confirmation of the influence of this parameter, thereby showing that low porous conductivity is well adapted to LHP applications in cases where high-power dissipation levels are required. A 3D model representing the entire length of the evaporator should contribute further details facilitating improved design for upcoming series of evaporators.

Acknowledgments

The authors acknowledge the funding of the INTAS Fellowship Grant for Young Scientists, Ref. No. 04-83-2885.

References

[1] Mike Ohadi, J. Qi, Thermal management of harsh-environment electronics, microscale heat transfer, fundamentals and applications, in: S. Kakac, L. Vasiliev, Y. Bayazitoglu, Y. Yener (Eds.), NATO Science Series, II Mathematics, Physics and Chemistry, vol. 193, Springer, Berlin, 2005, pp. 479–498.
[2] L.L. Vasiliev, Micro and miniature heat pipes – electronic component coolers, Appl. Therm. Eng. 28 (4) (2008) 266–273.
[3] D. Khrustalev, A. Faghri, Estimation of the maximum heat flow in the inverted meniscus type evaporator of the flat miniature heat pipe, Int. J. Heat Mass Transfer 39 (9) (1996) 1899–1909.
[4] D. Khrustalev, A. Faghri, Heat transfer in the inverted meniscus type evaporator at high-heat fluxes, Int. J. Heat Mass Transfer 38 (16) (1995) 3091–3101.
[5] T. Ogushi, H. Ishikawa, A. Yao, A. Miyasaka, H. Noda, Mathematical Modeling for Predicting Steady State and Transition Characteristics of Reservoir Embedded Loop Heat Pipe, 2001, SAE Paper No. 2001-01-2239.
[6] Yu. F. Maydanic, Loop heat pipes, Appl. Therm. Eng. 25 (5–6) (2005) 635–657.